Analytical Design and Analysis of Line-Start Permanent Magnet Synchronous Motors

Dan STOIA, Mihai CERNAT
Department of Electrical Engineering
Transilvania University of Brasov
Brasov, Romania
m.cernat@unitbv.ro

Adisa A. JIMOH, Dan V. NICOLAE
Department of Electrical Power
Tshwane University of Technology
Pretoria, South Africa
jimohaa@tut.ac.za

***Abstract*—The Line-Start Permanent Magnet Synchronous Motor (LSPMSM) attracted a considerable attention because of the higher value of the product between the power factor and the efficiency. The paper proposes an analytical design method for the LSPMSM, considering the asynchronous starting and the synchronous steady state parameters. Using this theoretical approach, all the synchronous and asynchronous starting characteristics will be calculated. The design of a motor having the following specifications: rated output power 3.5 kW, rated voltage 200 V, rated frequency 50 Hz, rated speed 3000 rpm is presented.**

Keywords—line-start synchronous motor, interior permanent magnet, design, analysis.

List of symbols

b_0 - slot opening;
B_{rem} - remanent magnetic flux density;
C_Φ - flux concentration factor;
D_M - mean PM diameter;
f - frequency;
F - mmf;
F'_a - rotor referred armature reaction mmf;
F_c - coercive mmf;
F_N - mmf corresponding to the PM operation point N;
F_t - tooth mmf;
F_δ - air-gap mmf;
i - armature current, instantaneous value;
i_D - damper current, instantaneous value;
I - armature current, rms value;
k_{ad} - armature reaction factor;
k_C - Carter's coefficient;
k_f - form factor of the excitation field;
k_{fd} - form factor of the armature reaction field;
k_{sat} - saturation coefficient;
k_w - stator winding factor;
$k_{\sigma M}$ - coefficient of the PM leakage flux;
l_M - PM length in the magnetization direction;
l_{Fe} - lamination stack length;
L_{ad} - self inductance;
L - synchronous inductance;
L_D - damper inductance;
L_m - magnetizing inductance;
L_σ - leakage inductance;
p - operator p=d/dt; p = j $s\,\omega_s$;
p - pole pair number;
P_{em} - electromagnetic power;
R - stator winding resistance;
R_D - damper (cage) resistance;
R'_D - stator referred damper (cage) resistance;
s - slip;
$s\,\omega_s$ - slip frequency;
S_M - PM cross section surface;
T - torque;
u - armature voltage, instantaneous value;;
U - stator voltage, rms value;
U_e - emf with armature reaction, rms value;
U_{eM} - emf without armature reaction, rms value;
X_a - armature reaction reactance;
X - synchronous reactance;
X_m - magnetizing reactance;
w - series stator winding turns per phase;
α_M - pole pitch coverage coefficient of the PM;
δ - air-gap length;
φ - load angle;
Φ - magnetic flux;
Φ_N, F_N - coordinates of the operation point N of the PM in flux-mmf coordinates;
Φ_{rem} - remanent magnetic flux;
Φ_δ - useful air-gap flux with armature reaction;
$\Phi_{\delta 0}$ - useful air-gap flux without armature reaction;
Λ - permeance
Λ_M - PM permeance;
Λ_δ - air-gap permeance;
Λ_σ - PM leakage permeance;
Λ_t - permanence of the external magnetic circuit;
μ_0 - vacuum permeability ($\mu_0 = 4\,\pi\,10^{-7}$ H/m)
μ_{rec} - recoil relative permeability ($\mu_{rec} = 1.02 \ldots 1.03$)
θ - internal angle of the synchronous motor;
τ_p - pole pitch length;
τ_s - slot pitch;
Ψ_a - armature reaction flux linked by the stator winding;
Ψ - flux linked by the stator winding;
Ψ_D - flux linked by the damper winding;
Ψ_{Mdu} - mutual flux between the PM and the stator winding;
ψ - power angle, angle between $\underline{U}_{eM}$ and $\underline{I}$ vectors;
ω_c - cage angular frequency;
ω_s - synchronous angular frequency of the motor;
Ω - geometrical synchronous angular speed
ξ - saliency ratio.

I. INTRODUCTION

Nowadays, the performance of permanent magnet (PM) materials has been highly improved and their prices are decreasing. Thus, PM synchronous motors are gradually used in many industrial applications for their high power factor, power density and efficiency [16, 17]. Standard PM motor architectures must be arranged to get the line-start property and to satisfy all the required qualities for various applications (pumps, fans, etc.). The line-start property is obtained thanks to rotor design.

The synchronizing process has been studied in literature [4-6], which indicates the effective parameters for reaching the starting capability, such as critical load torque, supply voltage, and back emf. The steady-state characteristics are also measured by different values of output power [1, 5, 8].

In this paper, an analytical method that considers the required starting performances and the steady-state performances which mainly depend on the size of the PM is obtained. The optimal size of PMs is the one which provides the required magnetic flux so that the reactive power exchanged with the power supply is minimal, to get a highest power factor which corresponds to the minimum line current. This behaviour is similar to the self-reactive power operation well known in wound synchronous motor and illustrated by Mordey's V-curves.

The designed motor has the following specifications: rated output power 3.5 kW, rated voltage 200 V, rated frequency 50 Hz, rated speed 3000 rpm.

II. THE OPERATING POINT OF THE PM

In general, a PM machine has a stator of a typical three-phase machine with semi-enclosed slots. The rotor contains an aluminium cage for asynchronous line starting and beneath buried rotor PMs made of NdFeB. The rotor has a non-magnetic material flux barrier on its quadrature axis to minimize the inter pole PM leakage flux.

A. The operating point of PM without armature reaction

Fig. 1 shows the equivalent circuit of the LSPM machine functioning without armature field.

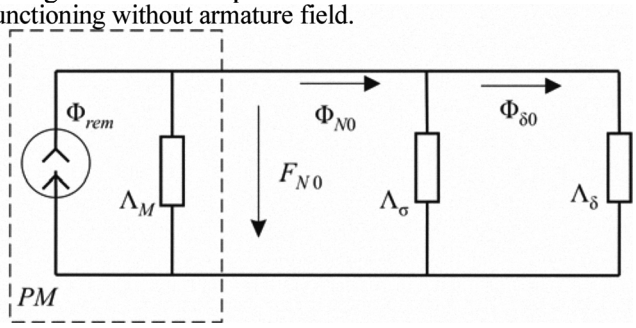

Figure 1. The equivalent circuit of the LSPM machine without armature reaction.

In Fig. 2 point N_0 is the operating point of the PM in the flux-mmf coordinates, which is at the intersection of the linear demagnetizing linear characteristic of the rare-earth PM and the load line (L_{l0}). In flux-mmf coordinates, the equations of (L_{rec}) line and (L_{l0}) line in Fig. 2 are [15]:

$$\Phi = \Phi_{rem} + \Lambda_M F; \qquad \Phi = -\Lambda_t F \qquad (1a, b)$$

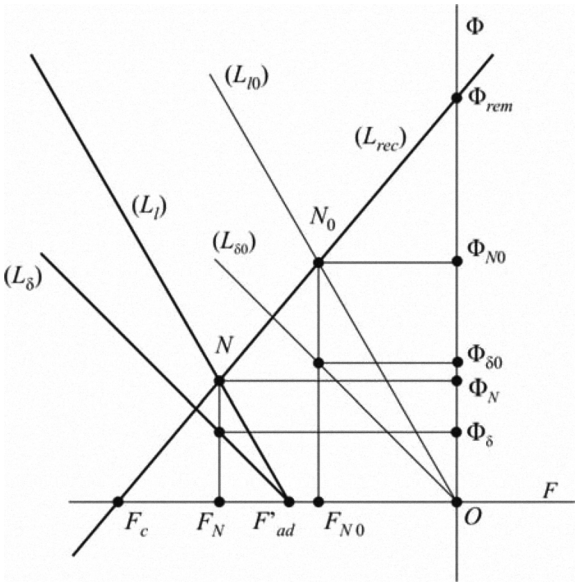

Figure 2. Determining of the operating point of the PM: Φ_{rem}- remanent flux; F_c – coercive mmf; (L_{rec}) - the recoil line, (L_{l0}) – the load line without armature field ; (L_l) – the load line with armature field; ($L_{\delta 0}$) and (L_δ) – the air-gap load line; N_0 – the operating point without armature field; N - the operating point with armature field.

respectively. Consequently, the coordinates of the operating point N_0 in flux-mmf coordinates (Fig. 2) are [15]:

$$\Phi_{N0} = \Phi_{rem} \frac{\Lambda_t}{\Lambda_t + \Lambda_M}; \quad F_{N0} = -\frac{\Phi_{rem}}{\Lambda_t + \Lambda_M} \qquad (2a, b)$$

where, from Fig. 1, the slope of the load line (L_{l0}) is:

$$\Lambda_t = \Lambda_\delta + \Lambda_\sigma \qquad (3)$$

The useful permeance Λ_δ corresponds to the useful flux in the active portion of the magnetic circuit. The leakage permeance Λ_σ is the referred leakage permeance of a single PM or of the PM with armature (in rotor and stator slots, the non-magnetic material and the air spaces between the magnet and the laminations). The PM permeance is:

$$\Lambda_M = \frac{\Phi_{rem}}{F_c} = \frac{B_{rem}\, S_M}{H_c\, l_M} = \frac{\mu_0\, \mu_{rec}\, S_M}{l_M} \qquad (4)$$

The air gap flux is

$$\Phi_{\delta 0} = \frac{\Lambda_\delta}{\Lambda_M / k_{\sigma M} + \Lambda_\delta} \Phi_{rem}; \qquad k_{\sigma M} = \frac{\Phi_M}{\Phi_{\delta 0}} > 1 \qquad (5)$$

The coefficient of the PM leakage flux is [12]

$$k_{\sigma M} = 1 + \frac{4\, l_M}{\pi\, \mu_{rec}\, \alpha_M\, \tau_p} \ln\left[1 + \frac{\pi\, \delta}{(1-\alpha_M)\, \tau_p}\right] \qquad (6)$$

The air gap permeance can be expressed as

$$\Lambda_\delta = (\alpha_M\, \tau_p\, l_{FE}\, \mu_0) / (\delta\, k_C) \qquad (7)$$

The Carter coefficient $k_C = k_{Cs} k_{Cr}$ can be calculated for the stator slots and for the rotor slots separately [12]:

$$k_{Cs} = \tau_{ss} / (\tau_{ss} - \gamma_s\, \delta) \qquad (8)$$

$$\gamma_s = \frac{4}{\pi}\left[\frac{b_{0s}}{2\,\delta} \operatorname{arc\,tg} \frac{b_{0s}}{2\,\delta} - \ln\sqrt{1 + \left(\frac{b_{0s}}{2\,\delta}\right)^2}\right] \qquad (9)$$

In this way, the air gap flux can be expressed as

$$\Phi_{\delta 0} = \frac{l_M}{l_M + \mu_r\, k_C\, k_{sat}\, k_{\sigma M}\delta}\,\Phi_{rem} \quad (10)$$

$$k_{sat} = (F_\delta + F_{ts} + F_{tr})/F_\delta \quad (11)$$

The back emf of the machine at no-load can be calculated for each speed (frequancy) from the following relation

$$U_{eM} = 4{,}44\, f\, w\, k_w\, \Phi_{\delta 0} \quad (12)$$

To minimize the machine volume, when the slot width and the tooth width are equal, the volume of PM results:

$$V_M = \alpha_M\, \tau_p\, l_{\mathrm{Fe}}\, l_M \quad (13)$$

B. The operating point of PM with armature reaction

Fig. 3 shows the equivalent circuit of the LSPM machine with armature reaction.

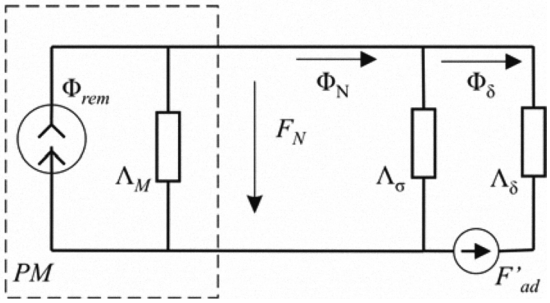

Figure 3. The equivalent circuit of the LSPM machine with armature reaction.

The armature field demagnetizes the PM, so that the new operating point *N* is obtained by translation of the N_0 point with the (*-F'ad*) which is the *d*-axis armature reaction mmf referred to the rotor (Fig. 2). In flux-mmf coordinates, the equations of (L_{rec}) line and (L_l) line in Fig. 2 are [15]:

$$\Phi = \Phi_{rem} + \Lambda_M\, F; \qquad \Phi = -\Lambda_t \left(F + F'_{ad}\right) \quad (14a, b)$$

respectively. Consequently, the coordinates of the operating point *N* in Fig. 2 are [15]:

$$\Phi_N = \frac{\Phi_{rem}\Lambda_t - \Lambda_M \Lambda_t F'_{ad}}{\Lambda_t + \Lambda_M};\; F_N = -\frac{\Phi_{rem} + \Lambda_t F'_{ad}}{\Lambda_t + \Lambda_M} \quad (15)$$

$$F'_{ad} = -\left(F_N + \Phi_N/\Lambda_t\right) \quad (16)$$

$$U_e = 4{,}44\, f\, w\, k_w\, \Phi_\delta \quad (17)$$

where Φ_δ is obtained from Fig. 4.

III. The Static Behaviour

The voltage equation of the machine is:

$$\underline{U} = \underline{U}_{eM} + R\underline{I} + \mathrm{j}\left(X_{ad}\,\underline{I}_d + X_{aq}\,\underline{I}_q + X_\sigma\,\underline{I}\right) \quad (18)$$

Correspondingly, it results the vector diagram in Fig. 4.

From the vector diagram the input current *I* can be resolved into components I_a and I_r, where I_a is the input active component (parallel to the voltage vector) and I_r is the lagging reactive component of input current.

After determining direct and quadrature components I_d and I_q onto the *r* axis (Fig. 4) on obtain

$$I = P_{em}/(\sqrt{3}\,U) = \sqrt{I_a^2 + I_r^2} = \sqrt{I_d^2 + I_q^2} \quad (19)$$

From the vector diagram (Fig. 4), by neglecting the armature resistance and the leakage reactance, $\theta = \psi - \varphi$ and the components of input current are [10]:

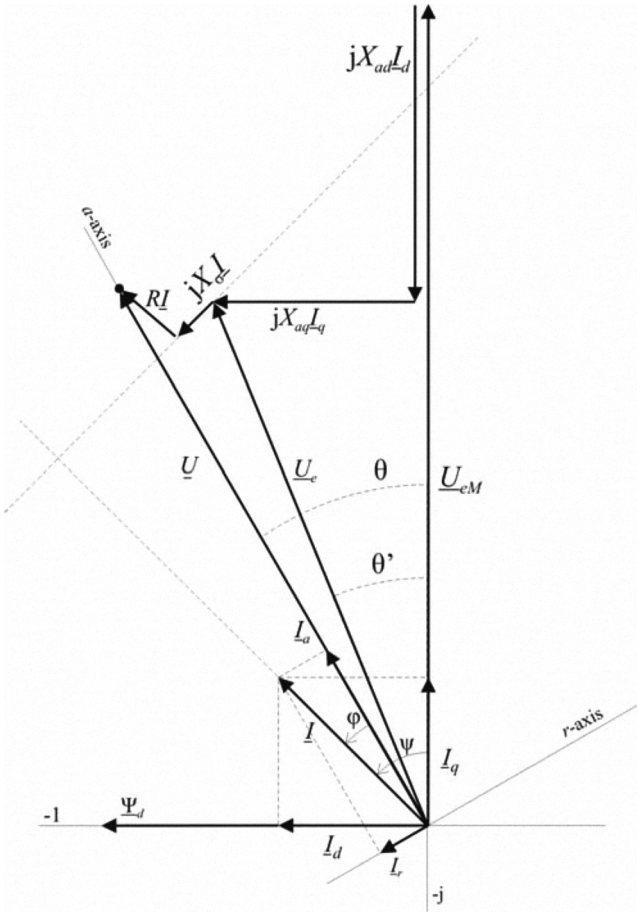

Figure 4. The vector diagram of the LSPM motor.

$$I_a = \left[\frac{U_{eM}}{X_{ad}} - \frac{U}{X_{ad}}\left(1 - \frac{X_{ad}}{X_{aq}}\right)\cos\theta\right]\sin\theta \quad (20)$$

$$I_r = -\left[\frac{U}{X_{ad}} - \frac{U_{eM}}{X_{ad}} - \frac{U}{X_{ad}}\left(1 - \frac{X_{ad}}{X_{aq}}\right)\cos\theta\right]\cos\theta \quad (21)$$

The loci of the armature current with increasing the armature voltage at no-load are the Mordey's V curves of the PM motor. For operating the machine at unity power factor, the voltage $U_{\lim}$ corresponding to the operating point of the V curve where the current I_0 is smallest, where the LSPM motor uses neither field weakening nor field strengthening is expressed as

$$U_{\lim} = \sqrt{U_{eM}^2 + (X_m I)^2} \quad (22)$$

$$X_m = 2X_{ad}\, X_{aq}/\left(X_{ad} + X_{aq}\right) \quad (23)$$

In this mode of operation, the input current locus

$$I = I_a\sqrt{1 + (I_r/I_a)^2} \quad (24)$$

is a circle that the no-load current is slightly loading.

IV. The Starting Process (Asynchronous Operation)

The equations of LSPM motor can be deduced from the Blondel dynamic model. In a *d-q* synchronous reference frame

the following set of equations is valid [10, 14]

$$u_d = R_d\, i_d + \mathrm{p}\,\Psi_d; \qquad u_q = R_q\, i_q + \mathrm{p}\,\Psi q$$
$$0 = \frac{R'_{Dd}}{s} i'_{Dd} + \mathrm{p}\,\Psi_{Dd}; \qquad 0 = \frac{R'_{Dq}}{s} i'_{Dq} + \mathrm{p}\,\Psi_{Dq} \tag{25}$$

The linkage fluxes in the above equations are defined by:

$$\begin{aligned}
&\Psi_d - \Psi_{Md} = \left(L_{ad} + L_\sigma\right) i_d + L_{ad}\, i'_{Dd} = L_d\, i_d + L_{ad}\, i'_{Dd}\\
&\Psi_q = \left(L_{aq} + L_\sigma\right) i_q + L_{aq}\, i'_{Dq} = L_q\, i_q + L_{aq}\, i'_{Dq}\\
&\Psi_{Dd} - \Psi_{Md} = L_{ad}\, i_d + \left(L_{ad} + L'_{Dd}\right) i'_{Dd}\\
&\Psi_{Dq} = L_{aq}\, i_q + \left(L_{aq} + L'_{Dq}\right) i'_{Dq}
\end{aligned} \tag{26}$$

From the above equations on obtain

$$\begin{aligned}
\Psi_d - \Psi_{Md} &= \left(L_d - \frac{\mathrm{p}\, L_{ad}^2}{R'_{Dd}/s + \mathrm{p}\, L'_{Dd}}\right) i_d = L_{dp}\, i_d\\
\Psi_q &= \left(L_q - \frac{\mathrm{p}\, L_{aq}^2}{R'_{Dq}/s + \mathrm{p}\, L'_{Dq}}\right) i_q = L_{qp}\, i_q
\end{aligned} \tag{27}$$

The operational impedances Z_{dp} and Z_{qp} of the LSPM motor, related to the power source are defined as

$$Z_{dp} = R + \omega_s L_{dp}; \qquad Z_{qp} = R + \omega_s L_{qp} \tag{28}$$

The input equivalent impedance is [10]:

$$\underline{Z} = R + \mathrm{j}\, X_\sigma + \frac{\left(R'_D/s + \mathrm{j}\, X'_{D\sigma}\right) \mathrm{j}\, X_m}{R'_D/s + \mathrm{j}\, X'_{D\sigma} + \mathrm{j}\, X_m} \tag{29}$$

In general, into the equation of the torque there are three components: the non-pulsating torque (average torque), which does not change with time, the first pulsating torque, which changes with time and slip frequency $s\,f$ and the second pulsating torque, which changes with time and double slip frequency $2\,s\,f$. During asynchronous operation, the rotating field passes on the magnet poles with the speed

$$n = (1 - s)\, 60\, f_s / p \tag{30}$$

The "synchronous part" of the LSPM machine sees the supplying network as a terminal short-circuit because of low values of the operational reactance at low frequency $s\omega_s$. In these conditions, the breaking torque will be associated with the stator copper losses because of the induced current created by the PMs [10]:

$$I_k = U_{eM} \frac{(1-s)\sqrt{(1-s)^2 X_q^2 + R^2}}{(1-s)^2 X_d\, X_q + R^2} \tag{31}$$

The active power generated by the short-circuit current is

$$P_k = 3\, R\, I_k^2 \tag{32}$$

By introducing the saliency ratio

$$\xi = X_q / X_d; \qquad \zeta = R / X_q \tag{33}$$

the power expressed by Eq. (32) produces the breaking torque:

$$T_{M\,br} = -\frac{3p}{2} \frac{(1-s)\, U_{eM}^2}{\omega_s} \frac{R}{X_q^2} \frac{(1-s)^2 + \zeta^2}{\left[(1-s)^2/\xi + \zeta^2\right]^2} \tag{34}$$

The slip value for obtaining the maximum breaking torque:

$$s_k = 1 - \zeta \sqrt{\frac{3}{2}(\xi - 1) + \sqrt{\frac{3}{2}(\xi - 1)^2 + \xi}}\,. \tag{35}$$

The expression for the cage torque can be written as [4]:

$$T_c = \frac{3p}{2} \frac{U^2\, X_m^2}{\omega_s} \frac{s\, R'_D}{a_1 + b_1 s + c_1 s^2} \tag{36}$$

$$a_1 = R_2'^2 \left[R_1^2 + \left(X_{\sigma 1} + X_m\right)^2\right]; \qquad b_1 = 2\, R\, R'_D\, X_m^2; \tag{37}$$

$$c_1 = \left(X_\sigma\, X_m + X'_{D\sigma}\, X_m + X_\sigma\, X'_{D\sigma}\right)^2 + R^2 \left(X_{\sigma 1} + X_m\right)^2.$$

$$R'_D = R'_{Dd} = R'_{Dq}; \qquad X'_{D\sigma} = X'_{D\sigma d} = X'_{D\sigma q}. \tag{38}$$

The electric speed at which the asynchronous torque is maxim is given by [4]:

$$\omega_c = s_k\, \omega_s = \omega_s \sqrt{a_1 / c_1} \tag{39}$$

Near synchronization, the slope of the damped oscillations is identified as [4]:

$$D = \frac{p}{2\, \omega_s\, s} \left(T_c - T_{M\,br} - T_l\right) \tag{40}$$

In starting process, the variety of armature current can be approximately divided into four stages (Figs. 5 and 6).

Stage one: *accelerating process*. The rotor accelerates from standstill. Due to the low speed, the slip is close to 1, the armature current is high and the electromagnetic torque is also high, thus the rotor runs with high acceleration.

Stage two: *approaching synchronizing process*. The speed rises continuously, and the slip is close to zero, but acceleration becomes lower and the armature current decreases significantly.

Stage three: *pulling into synchronization period.* The motor goes into the damped oscillation procedure.

Stage four: *synchronous operation period.* The waveforms of the armature current tend towards stabilization after several oscillations.

For the purpose of obtaining a higher value of the product between the power factor and the efficiency under load operation, the main value of input voltage must be lower than its rated value (135 V versus 200 V)

For the design purpose, the cage resistance is relatively high and the motor will produce high-starting torque even under low starting current. However, increasing the rotor resistance has a beneficial effect on the early start. On the other hand, the higher rotor resistance means that the slope of the asynchronous torque near the synchronous speed is very low. Due to the presence of the magnet braking torque, which is proportional to the square of the no-load voltage, the effective slope or the damping constant D has a value that is much dependent on the no-load voltage. An increase of the no-load voltage can lead to a reduced critical load torque. An optimum can be found for the no-load voltage to maximize the critical load torque.

Note that the decreasing of the volume of the PMs gives a better synchronization capability of motor with high power factor.

On the other hand, the value of the back emf of the PM affects the value of the reactance X_m. Increasing the amount of

magnets increases the no-load voltage and decreases the magnetizing reactance. Therefore, for the design motor increasing the volume of magnet gives a better synchronization capability but a lower critical load torque.

V. THE STEADY STATE (SYNCHRONOUS OPERATION)

At synchronous operation, the main torques that rotate the LSPM motors combine the PM alignment torque T_{PM} and the synchronous reluctance torque T_r. It is found that the synchronous loading capability is deeply influenced by the magnets' features such as the back emf and the reactance. The PM alignment torque is generated by the PMs and affected by the back emf and the q-axis current. With the design of different inductance of d-axis and q-axis an additional reluctance torque is provided, proportional to the difference between the d-axis and the q-axis reactances.

$$T_{em} = T_{PM} + T_r = \frac{3\,p}{2\,\omega} U_{eM} I_q + \frac{3\,p}{2\,\omega}\left(X_d - X_q\right) I_d\, I_q \qquad (41)$$

So, the electromagnetic torque of the LSPM motor can be expressed as

$$T_{em} = \frac{3\,U_{eM}\,U}{\Omega\,X_d}\sin\theta - \frac{3\,U^2}{2\,\Omega}\left(\frac{1}{X_d} - \frac{1}{X_q}\right)\sin 2\theta \qquad (42)$$

$$T_{em} = \frac{3\,U_{eM} I}{\Omega}\cos\psi + \frac{3}{2\,\Omega}\left(X_d - X_q\right) I^2 \sin 2\psi \qquad (43)$$

VI. THE STATIC STABILITY OF THE LSPM MOTOR

For a static stability of the machine at unity power factor operation, on are defined the power angle ψ between the U_{eM} and I vectors [13]:

$$\psi = -\arcsin\frac{U_{eM} - \sqrt{U_{eM}^2 - 4\,(X_d - X_q) X_q\, I^2}}{2\,(X_d - X_q)\,I} \qquad (44)$$

The limit value of the load angle have to satisfy the condition $\theta_{\lim} > \frac{\pi}{2}$, which can be achieved from

$$\cos\theta_{\lim} = -k + \sqrt{k^2 - 0.5}; \quad k = \frac{1}{4}\frac{U_{eM}}{U}\left(\frac{X_q}{X_d - X_q}\right) < 0 \qquad (45)$$

VII. ANALYSIS OF THE DESIGNED LSPMSM

Table I shows the numerical values of the design parameters of the designed LSPMSM. With these parameters, by applying Eqs. (20), (21) on obtain the Mordey's V curve at no-load operation. From the V curve of the designed motor, the value of U_{lim} can be obtained.

The condition of a good starting capability with a high value of the product between the power factor and the efficiency at load operation is [4]:

$$U_{eM} \cong 0.93\, U_{\lim} \qquad (46)$$

During the acceleration time interval of the starting process, the slip is high (from 1 to 0.6), the frequency of the rotor current is also high, the average cage torque is positive and contributes to rotor acceleration, while the average PM torque is negative and acts as a brake.

The armature current I, the induced current I_k, the input impedance and the components of the torque have the values indicated in Table II.

TABLE I. THE PARAMETERS OF THE DESIGNED LSPMSM.

Rated voltage, rms value [V]	U_N	135
Rated current, rms value [A]	I_N	10
Stator resistance [Ω]	$R_d = R_q = R$	0.675
Cage (damper) resistance [Ω]	$R'_{Dd} = R'_{Dq} = R'_D$	0.675
Stator leakage reactance [Ω]	$X_{\sigma d} = X_{\sigma q} = X_\sigma$	0.278
Cage leakage reactance [Ω]	$X'_{D\sigma d} = X'_{D\sigma q} = X'_{D\sigma}$	0.237
Magnetizing reactance [Ω]	X_m	5
Saliency ratio	ξ	1.1
Number of stator slots	Z_1	30
Number of rotor slots	Z_2	22
Lamination stack length [mm]	l_{Fe}	90
PM length [mm]	l_M	6
Mean PM diameter [mm]	D_M	90
Air-gap length [mm]	δ	0,8

TABLE II. VALUES OF FUNCTIONING PARAMETERS FOR $s \in [0.6, 1]$

s	I [A]	I_k [A]	T_c [Nm]	T_b [Nm]	Z_p [Ω]
1	58	0	24.0	o	0.734
0.9	57	14.0	24.0	-3.15	0.740
0.8	53	17.5	23.5	-6.00	0.742
0.7	51	18.5	22.0	-5.00	0.750
0.6	43	20.0	20.0	-4.00	0.756

TABLE III. VALUES OF FUNCTIONING PARAMETERS FOR $s \in [0.3, 0.5]$

s	I [A]	I_k [A]	T_c [Nm]	T_b [Nm]	Z_p [Ω]
0.5	25	19.5	18.2	-2.5	0.78
0.4	23	19.5	16.5	-2.1	0.81
0.3	20	19.7	14.5	-2	0.82

When the slip value becomes less than $s = 0.6$, the pull-in effect of the synchronization occurs, acceleration becomes lower and correspondingly the armature current decreases rapidly (Table III).

When the slip value becomes less than $s = 0.3$, the motor goes into the damped oscillations. When the slip is less than $s = 0.25$ the value of the input impedance becomes very high $Z_p = 20\ \Omega$, and the rotor is accelerated up to the synchronous speed, mainly by the PM torque.

When the slip is less than $s = 0.3$ the value of the input impedance becomes very high $Z_p = 20\ \Omega$, and the rotor is accelerated up to the synchronous speed, mainly by the PM torque. At $s = -0.2$ the value of the PM torque is $T_{PM} = 5$ Nm. The cage torque becomes oscillating with a zero mean value.

After the synchronization, the cage torque and the braking torque approach small values but not zero. The induced current is $I_k = 20$ A, the PM torque is $T_{PM} = 1.25$ Nm, and the cage torque is $T_c = 0.3$ Nm because the d- and q-axes reactances are about the same value.

The computed values of the steady state main parameters are: $T_{em\,\max}$=31.74 Nm, $T_{em\,n}$ =11 Nm, $I_{\max}$=17.8 A; θ_{n0}=20°; $\theta_{\lim}$=98°; cos φ=0.992.

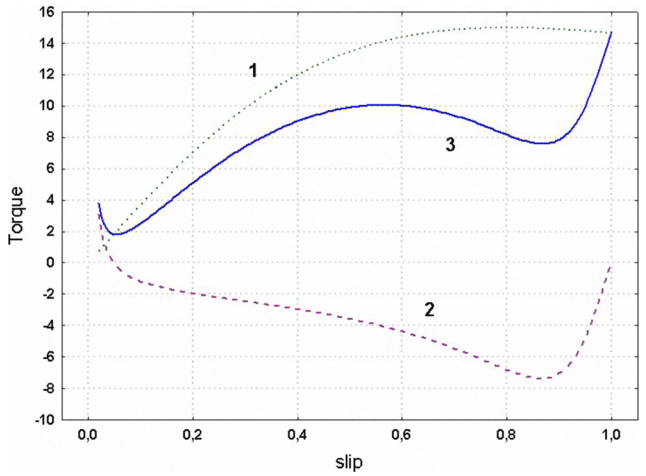

Figure 5. Cage torque (1), braking torque (2) and average torque (3) of the designed LSPMSM.

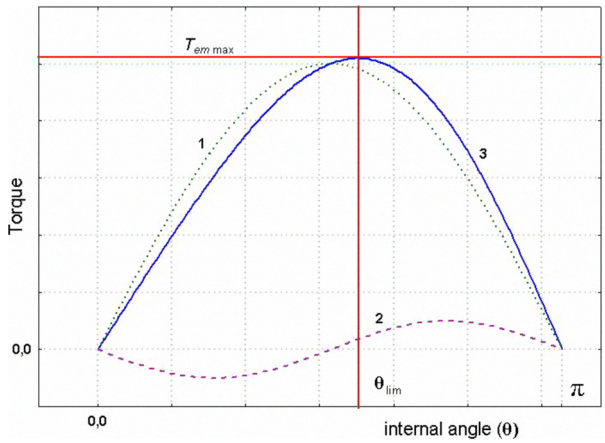

Figure 6. The synchronous torque and the reluctance torque of the designed LSPMSM.

VIII. CONCLUSION

An analytical design method for the LSPMSM, considering the asynchronous starting and the synchronous steady state parameters was proposed. Using this theoretical approach, all the synchronous and asynchronous starting characteristics can be calculated. In order to improve the starting capability of the LSPM motors, the main parameters that can be changed in the design are the rotor resistance, *d*- and *q*-axes reactances and the no-load voltage.

The volume of the PMs mainly rely on the following factors: the maximal energy product of magnets; the operating point and the torque-current ratio which the motor requires; the magnitude of back emf; the leakage coefficient; the magnetic saturation.

The LSPM designer has to find many compromises in the design process:

- the compromise between the value of starting torque, which depends mainly on the squirrel-cage design and material, and the starting current;
- the compromise between the value of braking torques (due to the presence of PMs in the asynchronous operating region) which depends mainly on the placement, dimensions and the value of energy product of PMs, which has the principal effect on the motor's synchronization capability;
- the compromise between an adequate starting characteristic in the asynchronous operating region and the torque capability and power factor × efficiency product in the motor's synchronous operating region.

REFERENCES

[1] D. Rodger, H.C. Lai, R.J. Hill-Cottingham, P.C. Coles, and F. Robinson, "A new high efficiency line start motor with high starting torque," Proc. Int. Conf. PEMD 2006, 4-6 April 2006, pp. 551–555.

[2] F. Libert, J. Soulard, and J. Engstrom, "Design of a 4-pole line start permanent magnet synchronous motor," Proc. ICEM 2002, Brugge, Belgium, Aug. 2002.

[3] G. Yang, J. Ma, J.X. Shen, Y. Wang, "Optimal Design and Experimental Verification of a Line-Start Permanent Magnet Synchronous Motor," Proc. ICEMS 2008, 17-20 Oct. 2008, pp.:3232 – 3236.

[4] J. Soulard and H.P. Nee, "Study of the synchronization of line-start permanent magnet synchronous motors," Proc. of 2000 IEEE Ind. Appl. Conf., Roma, 8-12 Oct. 2000, vol. 1, pp. 424–431.

[5] K. Kurihara and A. Rahman, "High-efficiency line-start interior permanent-magnet synchronous motors," IEEE Trans. Ind. Appl., vol. 40, no. 3, May/Jun. 2004, pp.789–796..

[6] I. Tsuboi, I. Hirotsuka, T. Takegami, and M. Nakamura, "Basic Concept of an Analytical Calculation Method and Some Test Results for Determination of Constant of Line Start Permanent Magnet Motor," Proc. ICEMS 2008, 17-20 Oct. 2008, pp. 3108-3111

[7] L. Zhiqiang, L. Yingli, L. Xiaofang, Z. Jian, "Pull out Torque Computation for Line Start Permanent Magnet Motor," Proc. ICEMS 2008, 17-20 Oct. 2008, pp.3270-3273.

[8] Q.F. Lu and Y.Y. Ye, "Design and Analysis of Large Capacity Line-Start Permanent-Magnet Motor," IEEE Trans. Magnetics, Vol. 44, No. 11, Nov. 2008, pp 4417-4420.

[9] W.H. Kim, K.C. Kim, S.J.Kim, et al., "A Study on the Optimal Rotor Design of LSPM Considering the Starting Torque and Efficiency," IEEE Trans. Magnetics, Vol. 45, No. 3, March 2009, pp. 1808-1811.

[10] V.B. Honsinger, "Permanent Magnet Machines: Asynchronous Operation," IEEE Trans. Power Apparatus and Systems, Vol. PAS-99, No. 4 July/Aug 1980, pp. 1503-1509.

[11] A. Levran, E. Levi, "Design of Polyphase Motors with PM excitation," IEEE Trans. Magnetics, Vol. MAG-20, No. 3, May 1984, pp. 507-515.

[12] M. Comanescu, A. Keyham, and Min Dai, "Design and analysis of 42-V permanent-magnet generator for automotive applications," IEEE Trans. Energy Conversion, Vol. 18, Issue 1, March 2003, pp. 107 – 112.

[13] G. Sturtzer, E. Smigiel, Modelling and control of three-phase motors (Modelisation et commande des moteurs triphases), Ellipses Edition, Paris, 2000.

[14] A.A. Jimoh, R.D. Findlay, "Parasitic torques in saturated induction motors," IEEE Trans. Energy Conversion, Vol. 3, Issue 1, March 1988, pp. 157 – 163.

[15] D.Ch. Karamousantas, G.E. Chatzarakis, G.N. Korres, P.J. Katsikas, "Obtaining State Equations for Planar Nondegenerate Linear Electric Circuits using Mesh Analysis with Virtual Voltage Sources," IJEEE (International Journal of Electrical Engineering Education), Manchester University, Vol. 45, No. 3, July 2008, pp. 239-250.

[16] D. Stoia, M. Antonoaie, D. Ilea, M. Cernat, "Design of Line Start PM Motors with High Power Factor," Proc. POWERENG 2007, Setubal, Portugal, 12-14 April 2007, published on CD-Rom, IEEE Catalog Number 07EX1654C, ISBN: 1-4244-0895-4, paper 186.

[17] D. Stoia, D. Ilea, M. Cernat, Al.B. Dezsi, A.A. Jimoh, "Stability of the Line-Start Permanent Magnet Synchronous Machine Sensorless Drive," Proc. 8th IEEE Africon Conference, Windhoek, Namibia, 26-28 Sept. 2007, published on CD-Rom, IEEE Catalog Number 07CH37876C, ISBN: 1-4244-0987-X, paper 639.

978-1-4244-3919-5/09/$25.00 ©2009 IEEE